Bioactive Materials 23 (2023) 551–562

Contents lists available at ScienceDirect

Bioactive Materials

journal homepage: www.keaipublishing.com/en/journals/bioactive-materials

Injectable bioorthogonal hydrogel (BIOGEL) accelerates tissue regeneration in degenerated intervertebral discs

Jeffrey Luo [a], Anjani Darai [b], Thanapat Pongkulapa [a], Brian Conley [a], Letao Yang [a], Inbo Han [b,**], Ki-Bum Lee [a,*]

[a] Department of Chemistry and Chemical Biology, Rutgers, The State University of New Jersey, Piscataway, NJ, 08854, USA
[b] Department of Neurosurgery, CHA University School of Medicine, CHA Bundang Medical Center, 59 Yaptap-ro, Bundang-gu, Seongnam-si, Gyeonggi-do, 13496, Republic of Korea

ARTICLE INFO

Keywords:
Bioorthogonal chemistry
Growth factor
Injectable hydrogel
Intervertebral disc degeneration
Tissue engineering

ABSTRACT

Intervertebral disc (IVD) degeneration is a leading cause of back pain and precursor to more severe conditions, including disc herniation and spinal stenosis. While traditional growth factor therapies (e.g., TGFβ) are effective at transiently reversing degenerated disc by stimulation of matrix synthesis, it is increasingly accepted that bioscaffolds are required for sustained, complete IVD regeneration. Current scaffolds (e.g., metal/polymer composites, non-mammalian biopolymers) can be improved in one or more IVD regeneration demands: biodegradability, noninvasive injection, recapitulated healthy IVD biomechanics, predictable crosslinking, and matrix repair induction. To meet these demands, tetrazine-norbornene bioorthogonal ligation was combined with gelatin to create an injectable **bio**orthogonal hydro**gel** (BIOGEL). The liquid hydrogel precursors remain free-flowing across a wide range of temperatures and crosslink into a robust hydrogel after 5–10 min, allowing a human operator to easily inject the therapeutic constructs into degenerated IVD. Moreover, BIOGEL encapsulation of TGFβ potentiated histological repair (e.g., tissue architecture and matrix synthesis) and functional recovery (e.g., high water retention by promoting the matrix synthesis and reduced pain) in an *in vivo* rat IVD degeneration/nucleotomy model. This BIOGEL procedure readily integrates into existing nucleotomy procedures, indicating that clinical adoption should proceed with minimal difficulty. Since bioorthogonal crosslinking is essentially non-reactive towards biomolecules, our developed material platform can be extended to other payloads and degenerative injuries.

1. Introduction

One of the most prevalent causes of back pain is intervertebral disc (IVD) degeneration. IVD degeneration is a progressive and irreversible process causing potential disability as a result of back pain (Fig. 1a) [1,2]. While growth factor injections have been investigated to encourage matrix synthesis in degenerated IVDs, these injections have not been clinically adopted due to poor efficacy [3]. More specifically, the short half-life of many growth factors [e.g., transforming growth factor beta (TGFβ, implicated in IVD extracellular matrix synthesis) has an *in vivo* half-life of 2–3 min] presents significant limitations to *in vivo* efficacy [3–5]. Fortunately, growth factors can be loaded into bioscaffolds, resulting in increased bioactivity by modulating release and safeguarding labile payloads from premature degradation [6]. In turn, bioscaffolds provide mechanical stability to the damaged area and act as a template for cells to reconstruct into healthy tissue, allowing the degenerated tissue to be efficiently repaired [6–10].

To effectively treat IVD degeneration, scaffolds should recapitulate the physicochemical properties of healthy IVD in a clinically translatable manner [11]. These scaffolds serve two key functions: i) regulating stress loading and reducing pain, and ii) delivering biophysical cues to promote pro-regenerative behavior [1,11]. Several FDA-approved IVD

Peer review under responsibility of KeAi Communications Co., Ltd.
* Corresponding author.
** Corresponding author.
E-mail addresses: hanib@cha.ac.kr (I. Han), kblee@rutgers.edu (K.-B. Lee).
URL: https://kblee.rutgers.edu/ (K.-B. Lee).
https://sites.google.com/view/inbolab/home (K.-B. Lee)

https://doi.org/10.1016/j.bioactmat.2022.11.017
Received 19 September 2022; Received in revised form 21 November 2022; Accepted 22 November 2022
Available online 12 December 2022

replacements are available, but they primarily comprise metal/synthetic polymer composites that neither recapitulate all biological functions nor mimic the viscoelastic mechanical properties of native IVD tissue [12–14]. While novel biomaterials are being explored for IVD regeneration, many mechanically robust synthetic polymers (e.g., polyethylene glycol, poly lactic-co-glycol acid) display poor biodegradability and/or poor cell adherence [2]. In contrast, various biopolymers (e.g., alginate, chitosan, gellan gum, decellularized IVD) rely on mechanically weak crosslinking modalities [15–17]. Among readily available biomaterials, gelatin-based hydrogels are well-suited for IVD treatment as they retain the unique combination of biocompatibility, biodegradability, cell adhesiveness, cell permissiveness, and viscoelastic properties of its parent structure collagen (a major component of healthy IVD tissue) [10,18–20]. While unmodified gelatin is unstable at physiological temperatures (i.e., melting at 37 °C), chemical modification with crosslinking groups can impart mechanical stability *in vivo* while retaining gelatin's beneficial biomaterial characteristics for IVD regeneration [10,18–20].

Among the many crosslinking modalities reported in the literature, bioorthogonal reactions are of special interest for biomedical applications [10,18,19,21]. These reactions form covalent bonds without damaging or interfering with endogenous tissues [10,21]. Tetrazine-norbornene ligation represents an ideal bioorthogonal system since these chemical moieties are absent in biological systems, exhibit high selectivity between the two functional groups, crosslink without external triggers or toxic byproducts, and remain stable in aqueous environments [10,21]. Moreover, tetrazine-norbornene ligation can be adapted to form *in situ* crosslinking hydrogels, which entail liquid precursors forming solid hydrogels within the body [10,19,22]. The clinical benefit of using bioorthogonal, injectable hydrogels for IVD regeneration includes minimizing damage to degenerated IVD tissue, lower costs, shorter post-operative recovery periods, and reduced surgical complications [10,22,23].

To address the above issues, we applied bioorthogonal chemistry to synthesize an injectable bioorthogonal hydrogel by grafting gelatin with tetrazine and norbornene groups (GelTz-Nb, BIOGEL) (Fig. 1b). The resulting BIOGEL system is ergonomic (e.g., it has a low viscosity, which allows for facile injection; it crosslinks within 10 min of mixing; and it changes color to indicate reaction completion) for ease-of-use in clinical settings, and it mimics the native IVD's biomechanical properties (e.g., viscoelasticity). This recapitulation of IVD biomechanical strength enables the BIOGEL scaffold to withstand mechanical stresses and remain intact until endogenous cells can infiltrate and remodel the hydrogel for

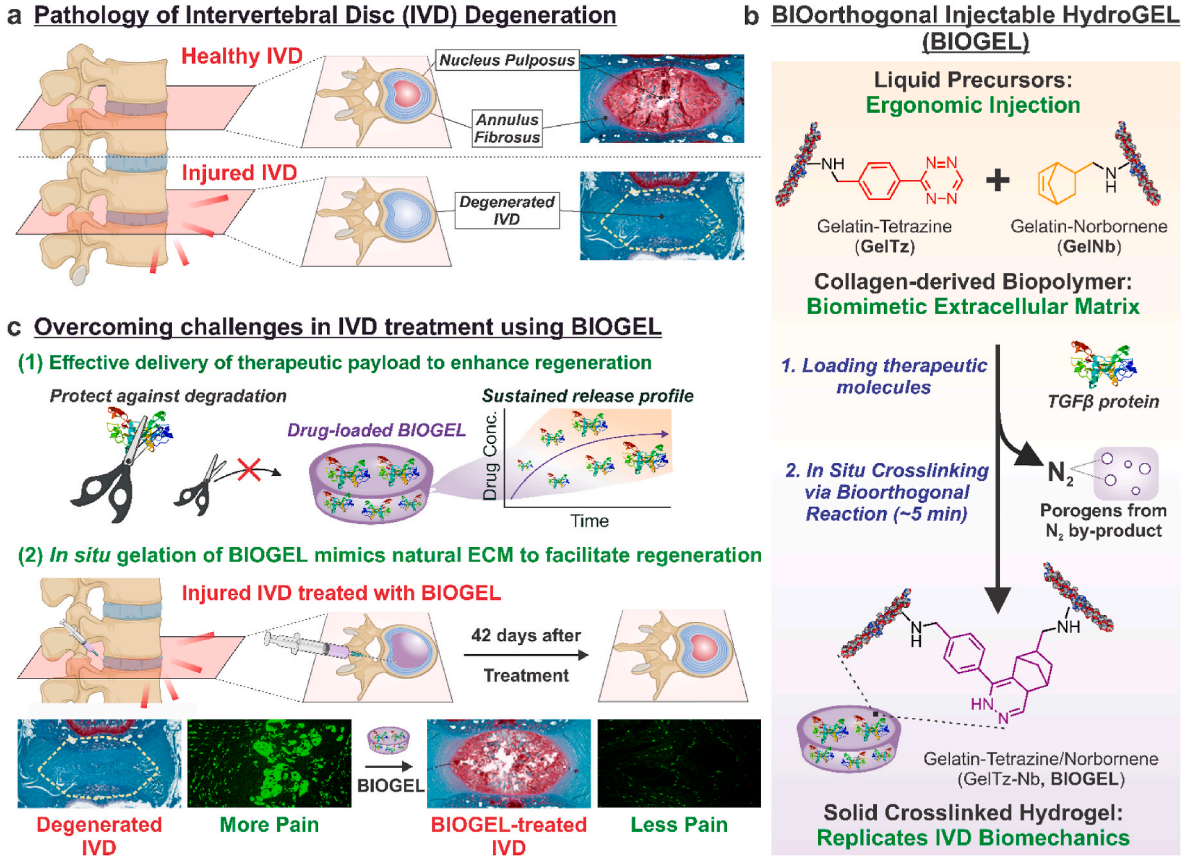

Fig. 1. Schematic for injectable bioorthogonal hydrogel (BIOGEL) for intervertebral disc (IVD) regeneration. a) IVD are load-bearing tissues found between two vertebrae. As a result of injury, genetic causes, or aging, IVD may enter a degenerative state whereby existing tissue damage causes improper stress transmittance, which encourages tissue breakdown. Bioscaffolds are highly suited to treat tissue breakdown caused by IVD degeneration. Such a therapy would ideally consist of a biocompatible, minimally invasive hydrogel to restore the integrity of IVD tissue. **b)** Gelatin-tetrazine (GelTz) and gelatin-norbornene (GelNb) are well-suited to form the basis for an injectable bioorthogonal hydrogel (BIOGEL). The bioorthogonal tetrazine and norbornene groups allow the liquid GelTz and GelNb precursors to form robust hydrogels approximately 5 min after simple mixing. Since the reaction is bioorthogonal (i.e., occurs under physiological conditions and does not react with endogenous biomolecules), this treatment can be combined with various therapeutic payloads and directly injected into patients to form minimally invasive hydrogels *in situ*. The resulting hydrogel is highly porous from the inert nitrogen gas byproduct, mimics native extracellular matrix (e.g., biocompatible, cell permissive), and mimics healthy IVD biomechanical properties. **c)** BIOGEL was adapted to treat IVD degeneration as a proof-of-concept. The role of BIOGEL was twofold: (1) to potentiate the effects of therapeutic payloads (e.g., TGFβ) and (2) facilitate regeneration. More specifically, BIOGEL encapsulation protects sensitive payloads from degradation and induces a sustained release profile over the course of regeneration. Additionally, BIOGEL regulates mechanical stresses and acts as a template for IVD regeneration. *In vivo* transplantation of the BIOGEL + TGFβ into injured IVD resulted in significant tissue regeneration, including restoration of healthy tissue architecture and enhanced IVD extracellular matrix secretion, to reduce discogenic pain.

IVD regeneration. Given the unique biological, chemical, and mechanical properties of BIOGEL, we adapted this injectable hydrogel system to address the need for effective IVD degeneration treatments. Our novel BIOGEL-based therapy included a pro-regenerative cytokine (TGFβ) and a scaffold that replicated IVD biomechanical properties to repair damaged IVD tissue (Fig. 1c) [2,3,11,24]. The injectable hydrogel can protect the labile payload from premature degradation, impart a sustained release profile, and undergo *in situ* gelation to mechanically reinforce the degenerated IVD. Meanwhile, TGFβ functions as a cell signaling cue to facilitate regeneration and remodel the scaffold [3,24].

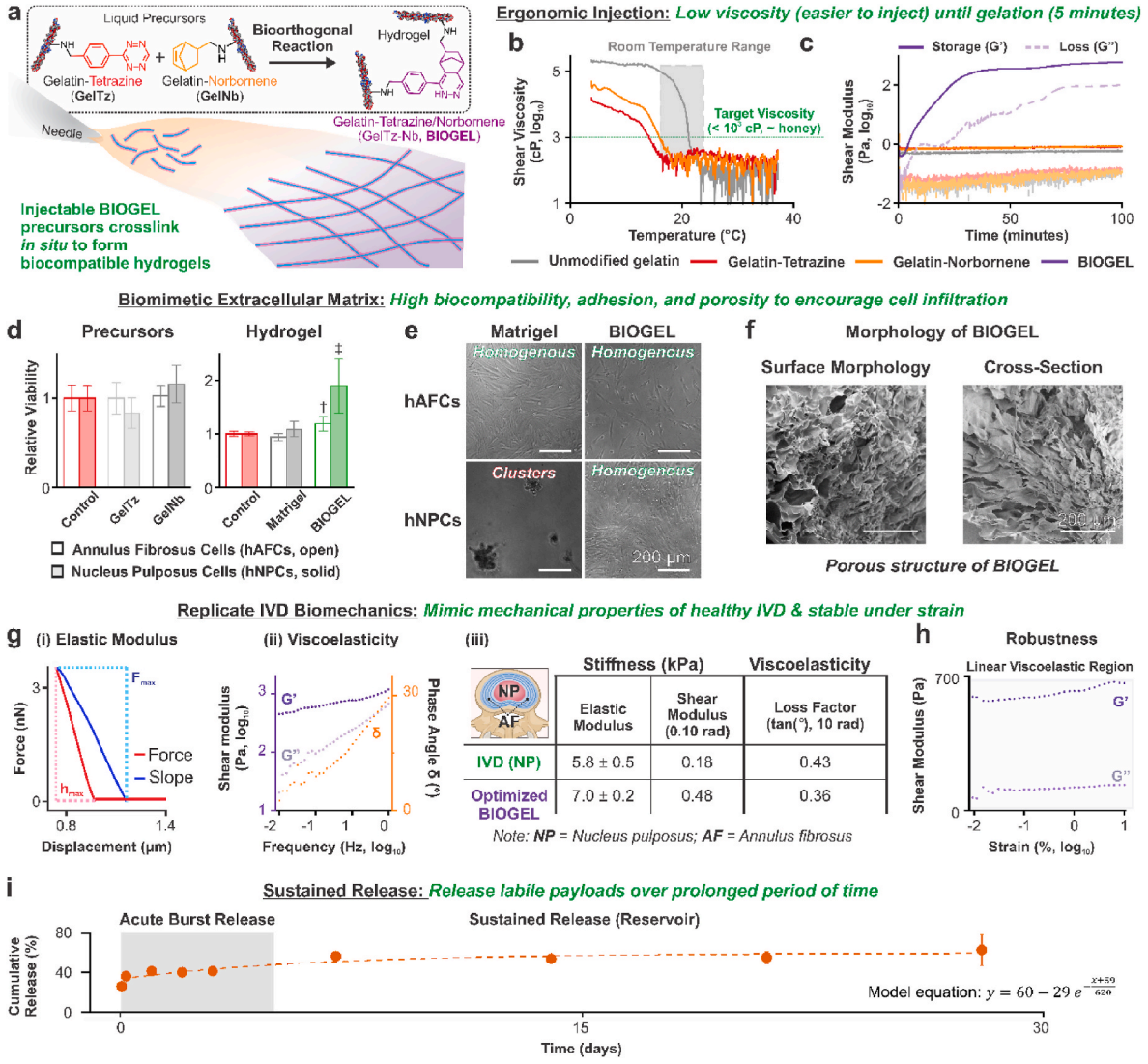

Fig. 2. BIOGEL recapitulates the biological and mechanical properties of healthy IVD tissue as an ergonomic, easy-to-use injectable hydrogel treatment. a) The BIOGEL injectable hydrogel system consists of two precursors, gelatin-tetrazine and gelatin-norbornene, which undergo *in situ* crosslinking after simple mixing. Since the underlying tetrazine-norbornene reaction mechanism is bioorthogonal, BIOGEL formation can occur with minimal interference from endogenous biomolecules. **b)** Precursor solutions were monitored for shear viscosity (typical room temperatures highlighted with a solid grey rectangle) at 1 Hz. Unmodified gelatin increased in viscosity at room temperature, reducing ease of injection and necessitating more force for injection. In contrast, GelTz and GelNb displayed low viscosity across a wide temperature range, indicating high injectability regardless of environmental conditions and greater preservation of shear stress-sensitive payloads (e.g., labile growth factors). **c)** Hydrogel crosslinking was monitored at 37 °C to simulate injection into a living patient. Precursor solutions do not exhibit any shear modulus increase, indicating no crosslinking. Only mixed GelTz-GelNb solutions (BIOGEL) experienced increased shear modulus and cross-linking. Gelatin initiation (sustained G′ increase) began approximately 5 min post-mixing with a plateau at approximately 95 min. **d)** In vitro culture of human primary IVD cells revealed that the precursor solutions are biocompatible. Moreover, cells undergo enhanced proliferation when seeded onto crosslinked BIOGEL substrates compared to PLL-coated tissue culture plastic control and Matrigel. **e)** BIOGEL was found to promote the homogenous distribution of seeded cells, whereas Matrigel induced cell clustering (IVD degeneration feature) in hNPCs. **f)** Under field-emission scanning electron microscopy, large pores exceeding most mammalian cell diameters were seen, indicating facile host cell infiltration. Such pores existed on the surface and interior of the hydrogel. **g)** To determine the biomechanical properties of BIOGEL, atomic force microscopy was used to determine the Young's modulus **(i)** while rheometry was used for shear modulus and phase angle **(ii)**. The results are summarized in table **(iii)**, where BIOGEL exhibited mechanical properties similar to that of native IVD tissue reported in the literature (IVD values obtained from Refs. [29,30]). **h)** BIOGEL retained its original mechanical properties even under significant strain (at least 10%), indicating high wear resistance and resiliency under mechanical load. **i)** Growth factors and other payloads (e.g., fluorescently labeled insulin) can be incorporated into the hydrogel by mixing with either precursor solution. Once the hydrogel is crosslinked, encapsulated payloads were released in a biphasic manner: an initial burst release followed by sustained release over time. This can be roughly modeled with an exponential decay function. Approximately 40% of the original loading mass remained within the hydrogel even after prolonged incubation. Relative viability was analyzed using one-way ANOVA followed by Dunnett's Test within cell groups [$\alpha = 0.05$; † and ‡ indicate a statistically significant difference against all other conditions with different symbols, $n = 5$ biological replicates].

This injectable hydrogel system was then adapted for nucleotomy procedures (removal of nucleus pulposus material through an annulus fibrosus incision) to demonstrate the ease of clinical translation [24,25]. Collectively, our TGF-loaded BIOGEL treatment was found to improve histological recovery (e.g., tissue architecture and proteoglycan synthesis), which translated into increased functional recovery (e.g., reduced pain) in animal IVD degeneration models.

2. Results and discussion

2.1. BIOGEL synthesis and physicochemical characterization

Gelatin was selected to form the injectable hydrogel since it retains many biological functions of its parent structure, collagen (a major component of healthy IVD tissue) [20]. Since gelatin melts at physiological temperatures, a crosslinking mechanism is required to impart stability during IVD regeneration [20]. Tetrazine and norbornene were chosen as the bioorthogonal functional groups because of their simple synthesis, favorable reaction kinetics, and essentially non-reactivity toward endogenous biomolecules [10,21]. Moreover, the crosslinking reaction generates non-toxic byproducts and is easily initiated by simple mixing [10]. The resulting gelatin-tetrazine (GelTz) and gelatin-norbornene (GelNb) is a shelf-stable solid that can be freely reconstituted. Once mixed, GelTz and GelNb solutions form the BIOGEL hydrogel at ambient temperatures without substantial interference from other biomolecules. This bioorthogonal reaction was adapted to form an injectable hydrogel system, where the liquid precursors are injected *in vivo* and allowed to crosslink *in situ* (Fig. 2a).

Gelatin natively contains functional groups for bioconjugation. Norbornene-Methylamine (5-norbornene-2-methylamine) is commercially available, while Tetrazine-Methylamine [4-(1,2,4,5-tetrazin-3-yl) phenyl)methanamine hydrochloride] synthesis (Fig. S1) and nuclear magnetic resonance (NMR, Fig. S2) are found in Supplementary Information [26]. GelTz and GelNb synthesis schematics are found in Fig. S3a. First, gelatin was modified with succinic anhydride to (1) increase available carboxylic acid groups for further modifications, (2) prevent amine-carboxylic acid cross-coupling within gelatin molecules, and (3) reduce shear viscosity of the resulting precursor solution. Carboxylic acid groups on the succinylated gelatin were conjugated with Tetrazine-Methylamine and Norbornene-Methylamine via carbodiimide chemistry to form GelTz and GelNb. NMR (Fig. S3b) confirmed the addition of succinate groups, tetrazine, and norbornene. The conjugated π-π system of Tetrazine-Methylamine gives GelTz a bright red color with an absorption maximum at 518 nm (Fig. S4a). This permits facile visualization of the injected hydrogel as it crosslinks, since the 518 nm peak diminishes as the reaction progresses (Figs. S4b–d). When tactile feedback is limited (e.g., laparoscopic surgeries), this additional means of verifying successful BIOGEL crosslinking is desirable to (1) indicate when mixed GelTz-Nb solution is no longer injectable and (2) confirm gelation once injected into the patient.

Ease of injection is paramount for an injectable hydrogel system, particularly considering constraints present in a surgical site (e.g., space for additional equipment). The injectable hydrogel should keep a low viscosity so that it can be easily delivered to the patient, the amount of force needed for injection can be minimized, and shear stresses can be reduced [7,8]. Biopolymers may exhibit significantly increased viscosity when placed in non-optimal conditions, thus hindering injection. Unmodified gelatin solutions became significantly more viscous at room temperature (Fig. 2b), potentially necessitating additional equipment to maintain physiological temperatures prior to injection [20]. GelTz and GelNb solutions exhibited low viscosities across a wider range of temperatures (e.g., honey at 37 °C has a viscosity of approximately 10^3 cP). These results were also seen when measuring the shear modulus of the precursor, whereby the GelTz and GelNb solutions exhibited lower moduli than gelatin or succinylated gelatin (Fig. S5). With a lower viscosity, less force is required to pass the precursor solutions through a syringe, and any encapsulated payloads (e.g., sensitive proteins or cells) will experience less damaging shear stresses during injection [7]. Thus, ease of injectability is maintained across a wide temperature range for the BIOGEL hydrogel system, and additional equipment is not required to maintain optimal injection temperatures.

Ergonomic design and use are important considerations when translating a new therapy to the clinic. A crosslinking-based injectable hydrogel must react at an appropriate timescale. Excessively fast reactions can be difficult when administering the hydrogel before complete gelation [6]. Unacceptably slow reactions can be subjected to premature clearance by local fluid flow and increase healthcare costs related to prolonged operations [6]. BIOGEL gelation (i.e., sustained increase in shear modulus) began approximately 5 min after precursor mixing with a plateau after 95 min (Fig. 2c). *In vivo* experiments were usually concluded (i.e., closing the surgical site) before the gelation plateau was complete. As a control, unmodified gelatin and individual precursor solutions were subjected to the same rheometer time sweep sequence and failed to achieve any substantial gelation. The delay in gelation was deemed appropriate for clinical use as it gave the operator ample time to thoroughly mix the precursor solutions, load into a syringe, and administer to the surgical site.

While tetrazine-norbornene ligation is bioorthogonal and BIOGEL uses a biomimetic extracellular matrix (ECM), it is still prudent to establish the cell adhesiveness, biocompatibility, and biodegradability of both the precursor solutions and BIOGEL. Cytotoxicity assays on human annulus fibrosus cells (hAFCs) and human nucleus pulposus cells (hNPCs) showed no significant cell death when (1) precursor solutions are compared to media or (2) BIOGEL is compared to conventional cell culture on poly-L-lysine (PLL)-coated tissue culture plastic control or Matrigel hydrogels (Fig. 2d). In fact, BIOGEL was found to promote hAFC and hNPC proliferation. When monitoring the morphology of cells on PLL, Matrigel, and BIOGEL, an interesting observation was seen in hNPCs. Matrigel induced hNPCs to form cell clusters, an *in vivo* indication of IVD degeneration, whereas cells on BIOGEL maintained conventional monolayer culture (Fig. 2e) [24]. In addition, crosslinked BIOGEL samples were verified to be biodegradable via collagenase digestion (Fig. S6). Lastly, both the BIOGEL precursors and hydrogel were also found to be non-toxic to human-induced pluripotent stem cell-derived neuronal progenitor cells (hiPSC-NPC, Fig. S7), indicating biocompatibility with neuronal tissue in the nearby spinal cord.

FE-SEM revealed that BIOGEL contained pores larger than 100 μm (the upper bound for most mammalian cells), even after dehydration for electron microscopy. These pores were seen both on the surface of the hydrogel and when it was cross-sectioned (Fig. 2f). Porous hydrogels are well-documented to promote nutrient exchange and encourage host cell infiltration and integration, thus providing resident cells with a favorable microenvironment to remodel the injectable hydrogel [7,9]. The combination of high biocompatibility, high cell adhesiveness, and high porosity enables host cells to readily infiltrate the hydrogel for eventual remodeling and tissue regeneration.

Since one of the key IVD functions is load transmission throughout the spinal column, the mechanical properties of BIOGEL are important for *in vivo* function. Similarity to healthy human IVD tissue is significant as it assists with regulating cellular mechanotransduction, host tissue integration, and normal loading bearing (i.e., lack of stress shielding) [27,28]. Atomic force microscopy (AFM) was employed to obtain a detailed image of BIOGEL when hydrated (Fig. S8) and to determine the elastic modulus (Fig. 2g–i), while rheometry was used to determine viscoelastic behavior under shear stresses (Fig. 2g–ii). BIOGEL exhibited elastic modulus, shear modulus, and loss factors similar to healthy IVD tissue (Fig. 2g-iii) [29,30]. In comparison, current FDA-approved treatments exhibit significantly higher elastic modulus than healthy IVD (e.g., elastic modulus on the order of GPa) [12–14]. Moreover, oscillatory frequency sweeps indicated that BIOGEL viscoelasticity allows for the overall structure to remain unchanged at low frequencies (elastic behavior) while undergoing dynamic reorganization in response

to high frequency (viscous behavior) [28]. In practice, this viscoelasticity allows the hydrogel to maintain its shape for low-frequency forces (e.g., standing at rest) and deform at higher frequencies (e.g., rapid spine extension and rotation). Additionally, the hydrogel retained its mechanical properties under a wide range of strains (0.01–10% strain, termed linear viscoelastic region), showing that the hydrogel does not undergo structural breakdown and has high wear resistance (Fig. 2h) [28]. Taken together, the BIOGEL system performs similarly to healthy IVD tissue under key mechanical loading situations expected when implanted *in vivo*.

2.2. BIOGEL enhances in vitro efficacy of growth factor therapy

While BIOGEL can provide mechanical support to degenerated IVD, it is preferable to concurrently induce nearby cells to remodel the hydrogel and regenerate damaged tissue. Growth factor therapies are suited to initiate IVD regeneration but suffer from significant issues that limit clinical efficacy [5]. For TGFβ, a well-known cytokine that is implicated in ECM remodeling and anti-inflammation, its short *in vivo* half-life severely limits its clinical potential as a bolus injection [3–5, 31–33]. Potential benefits may be found by encapsulating TGFβ with the BIOGEL system to reverse IVD degeneration.

The release of encapsulated payloads in BIOGEL was modeled using FITC-labeled insulin (similar size to TGFβ). Since GelTz and GelNb can be dehydrated into a shelf-stable solid, FITC-insulin was integrated into the hydrogel by reconstituting GelTz in a FITC-insulin solution. A biphasic release profile was seen where burst release within the first five days transitions into a more gradual, sustained release (Fig. 2i, S9). This biphasic drug release behavior persisted under various physiological conditions including tissue acidosis, alkalosis, hypothermia, and hyperthermia (Fig. S10). Moreover, a portion of FITC-insulin (approximately 40% of the original loading mass) remained trapped in the

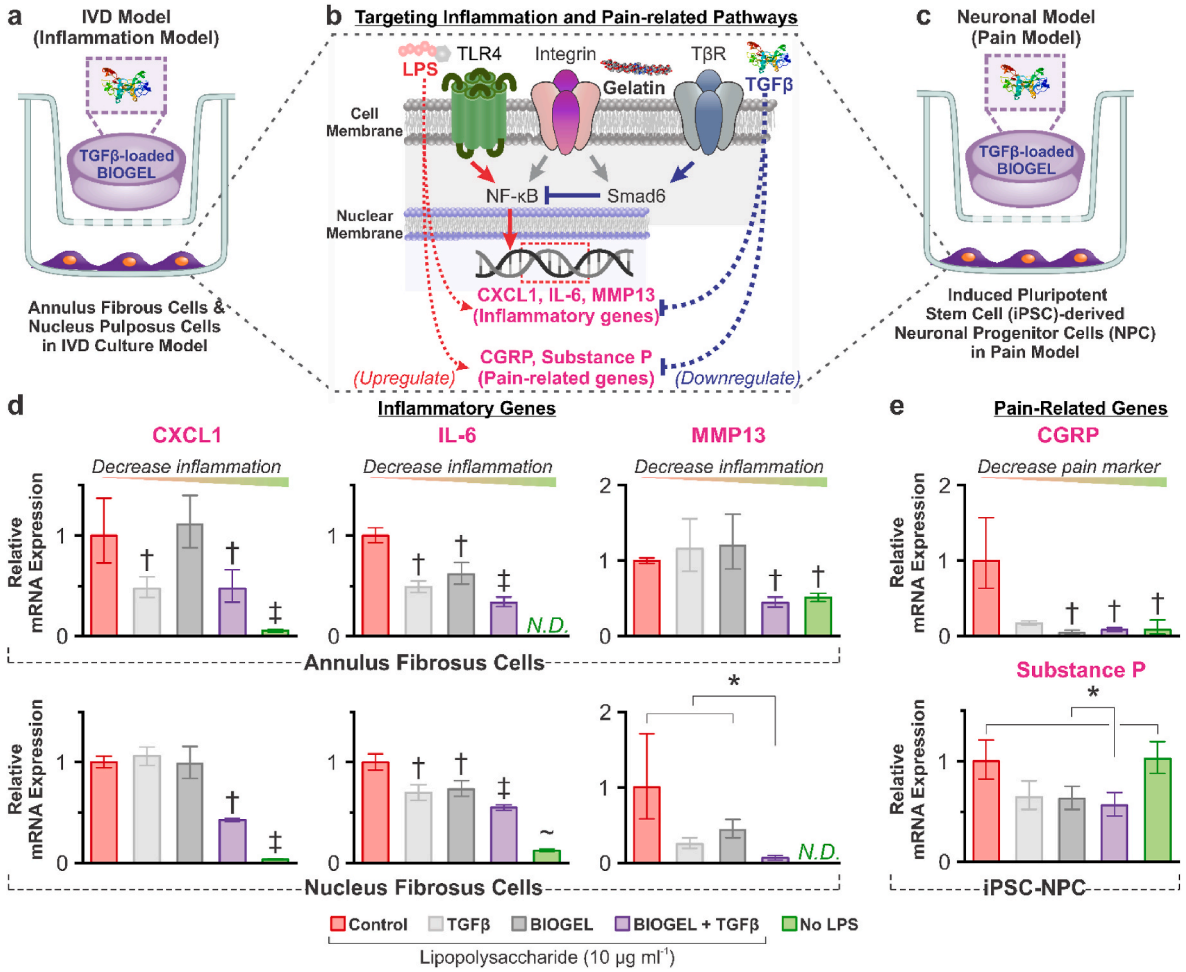

Fig. 3. BIOGEL acts as a reservoir of pro-regenerative, anti-inflammatory payloads for the in vitro model of IVD degeneration. a) Schematic diagram of in vitro IVD degeneration model using primary human annulus fibrosus cells (hAFCs) and nucleus pulposus cells (hNPCs). TGFβ-supplemented media, bare BIOGEL, and TGFβ-loaded BIOGEL (TGFβ-BIOGEL) were administered via tissue culture inserts and incubated for 24 h. **b)** To induce an inflammatory phenotype and stimulate degenerative pathways, lipopolysaccharide (LPS) was administered to induce NF-κB activity. This increased expression of various inflammation and pain-related genes such as C-X-C Motif Chemokine Ligand 1 (CXCL1), Interleukin-6 (IL-6), Matrix Metalloprotease 13 (MMP13), calcitonin gene-related peptide (CGRP), and Substance P. TGFβ acts as an anti-inflammatory cytokine by activating Smad6, which blocked NF-κB activity, thus reducing the expression of pro-inflammatory and pain-related genes. Free, unreacted gelatin from BIOGEL can activate integrin pathways which influence both pro-inflammatory and anti-inflammatory pathways. **c)** Human-induced pluripotent-derived neuronal progenitor cells (hiPSC-NPC) were also explored with this degeneration system with an additional neuronal differentiation step before LPS stimulation. **d)** After LPS exposure, both hAFCs and hNPCs experienced significantly increased expression of pro-inflammatory cytokines (CXCL1, IL-6, and MMP13). While TGFβ and BIOGEL led to statistically significant decreases in some genes, only TGFβ-BIOGEL led to consistent decreases in all three pro-inflammatory genes, indicating encapsulation of TGFβ within BIOGEL potentiates its anti-inflammatory effect. **e)** While LPS was insufficient at upregulating Substance P in this hiPSC-NPC cell line, TGFβ-BIOGEL was found to be effective at mitigating pain-related markers (CGRP and Substance P). RT-qPCR was analyzed using one-way ANOVA followed by Tukey's HSD [$\alpha = 0.05$, * indicates a statistically significant difference; †, ‡, and ~ indicates a statistically significant difference against all other conditions with different symbols, n = 3 biological replicates].

hydrogel under normal physiological conditions. The presence of unreleased payload (e.g., TGFβ) represents a significant benefit over conventional growth factor therapies. Whereas injected TGFβ has a short half-life and is rapidly cleared, a significant portion of TGFβ within the hydrogel is sequestered until cells infiltrate and release the trapped payload [3–5,24]. BIOGEL protects against premature clearance and acts as a reservoir of sequestered TGFβ, while the growth factor induces cells to remodel the hydrogel, abate pro-inflammatory signals in the environment, and initiate pro-regenerative cascades [3,5,6].

To verify the BIOGEL system's capacity to enhance growth factor therapies, hAFCs, hNPCs, and differentiated hiPSC-NPC neurons were treated with lipopolysaccharide (LPS) to simulate an inflammatory state comparable to IVD degeneration (Fig. 3a) [34,35]. In hAFCs and hNPCs, this testing condition promotes the production of IVD degeneration

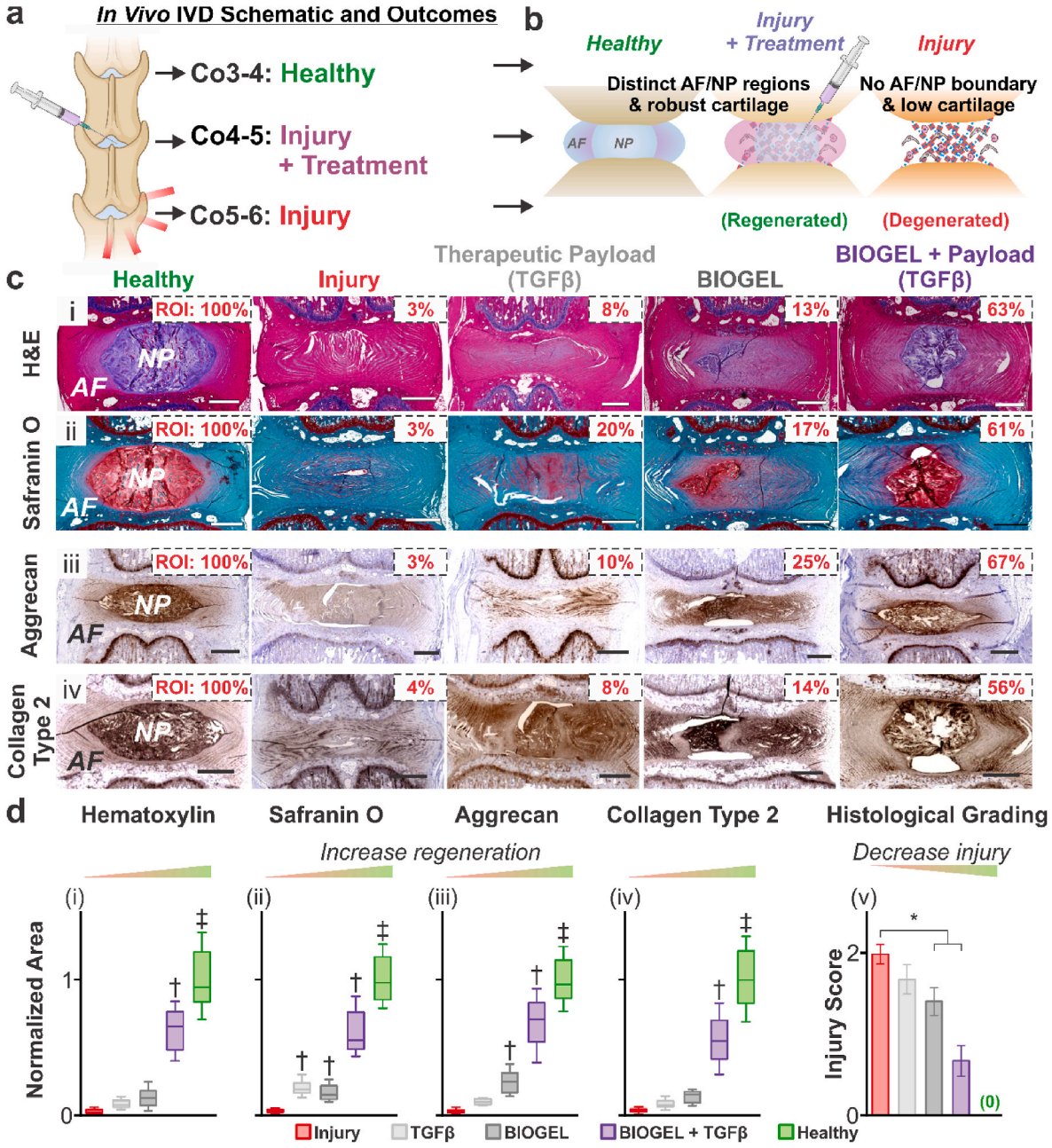

Fig. 4. Injectable TGFβ-loaded BIOGEL promotes IVD tissue histology regeneration after injury. a) Schematic diagram of *in vivo* IVD degeneration model. Nucleotomies were performed on the Co4-5 and Co5-6 IVD of Sprague-Dawley rats. Immediately after nucleotomies, TGFβ solution, BIOGEL, and TGFβ-loaded BIOGEL were injected into the Co4-5 nucleus pulposus void space. Co3-4 IVD were used as a healthy control. **b)** Healthy IVD was defined by distinct nucleus pulposus and annulus fibrosus boundaries, with the nucleus pulposus containing ample collagen type 2, aggrecan, and assorted proteoglycans. **c)** Fixed IVD sections were stained with **(i)** hematoxylin & eosin and **(ii)** Safranin O (fast green counterstain) along with immunohistochemistry staining for **(iii)** Aggrecan and **(iv)** Collagen type 2. **d)** Staining area for **(i)** hematoxylin, **(ii)** Safranin O, **(iii)** Aggrecan, and **(iv)** Collagen type 2 was normalized to healthy, uninjured IVD. Out of all treatment conditions, only TGFβ-loaded BIOGEL resulted in statistically significant increased staining across all targets. Additionally, TGFβ-loaded BIOGEL led to the greatest recovery of staining among treatment conditions. Further holistic quantification of IVD injury/degeneration **(v)** indicated TGFβ-loaded BIOGEL induced the greatest histological recovery. Staining and histological grading were analyzed using one-way ANOVA followed by Tukey's HSD [$\alpha = 0.05$, * indicates a statistically significant difference, † and ‡ indicates a statistically significant difference against all other conditions with different symbols, treatments: n = 8 biological replicates, healthy and injury: n = 24 biological replicates (i.e., 8 from each treatment group)].

markers such as C-X-C Motif Chemokine Ligand 1 (CXCL1), Interleukin-6 (IL-6), and Matrix Metalloprotease 13 (MMP13) (Fig. 3b) [36]. Similarly, hiPSC-NPC neurons express pain-related genes such as calcitonin gene-related peptide (CGRP) and Substance P (Fig. 3b and c) [37]. These LPS-activated signaling pathways can be blocked by administering TGFβ to induce anti-inflammatory cascades, leading to reduced IVD degeneration and pain [32,33]. While free, unreacted gelatin is well-known for activating integrin receptors, its net effect on inflammation is less predictable as it can activate both pro- and anti-inflammatory pathways [38].

TGFβ solution, bare BIOGEL, and TGFβ-loaded BIOGEL (TGFβ-BIOGEL) were administered to LPS-primed cells via cell culture inserts (0.4 μm pore to allow diffusion from the treatment chamber to cells) to test their ability to mitigate the pro-inflammatory, pain-inducing effects of LPS (Fig. 3a,c). After 24 h, the various inflammatory and pain markers were found to be significantly reduced when cells were treated with TGFβ-BIOGEL (Fig. 3d and e). Though the reduction usually could not achieve gene expression levels found in the non-inflammatory control, these showed significant potential for TGFβ-BIOGEL to reduce IVD degeneration and pain. Moreover, TGFβ-BIOGEL was found to reduce inflammatory and pain markers with similar or greater efficiency than either TGFβ or BIOGEL component by itself, suggesting that BIOGEL encapsulation potentiates therapeutic payload effects. While LPS was insufficient at inducing Substance P upregulation here, the ability of TGFβ-BIOGEL to downregulate baseline expression is significant enough to warrant interest in IVD treatment.

Several ECM-related genes were also assayed in hAFCs and hNPCs (i.e., Aggrecan, Collagen Type 2) but failed to yield sufficient PCR amplification (data not shown). Dedifferentiation and loss of ECM-related gene expression are well documented for primary IVD cells after extended monolayer culture [39].

2.3. BIOGEL enhances In vivo histological recovery

IVD degeneration is a complex pathology that necessitates *in vivo* experiments to assess novel therapies. Nucleotomy (removal of nucleus pulposus material [NP] through an annulus fibrosus [AF] incision) was selected as the IVD degeneration model and method of BIOGEL injection due to established clinical use in conditions such as lumbar microdiscectomy, which is the most commonly performed spinal surgery procedure [25]. Sprague Dawley rats were subjected to nucleotomies at coccygeal vertebrae 4–5 and 5–6 (Co4-5 and Co5-6), with Co4-5 receiving TGFβ, BIOGEL, or TGFβ-loaded BIOGEL treatments. Co3-4 was designated as the non-injured control. Forty-two days after treatment, the rats were sacrificed for tissue harvesting and histological assessment of the IVD (Fig. 4a). Healthy IVD tissue contains distinct boundaries between the AF and NP, while degenerated IVD lacks a clear boundary [24]. Hematoxylin and Eosin (H&E) staining was used to visualize this boundary as the interface between the pink, eosinophilic AF and purple, hematoxylin-staining NP [24,40]. Additionally, proteoglycan-rich NP stains red, while the AF stains blue-green under Safranin-O/Fast Green [24,40]. Together, these staining techniques were used to elucidate the extent of IVD regeneration (Fig. 4b).

Healthy IVD discs retained distinct AF/NP regions, while injured IVD showed diminished boundaries. While TGFβ and bare BIOGEL, as control conditions, in the Co4-5 IVD showed negligible to modest recovery of AF-NP boundaries, TGFβ-loaded BIOGEL displayed substantial histological recovery as quantified by hematoxylin and Safranin O-stained area (Fig. 4c,d-i,ii) and histological grading (Fig. 4d-iii). The recovery of distinct AF/NP boundaries and proteoglycan content in the NP indicated regeneration [24,40]. More specifically, the recovered proteoglycan content helped the IVD retain water and resist compressive forces during load bearing [11]. Since BIOGEL contained fewer proteoglycans than the TGFβ-loaded BIOGEL, we conclude that the injected BIOGEL potentiates encapsulated growth factor therapies (e.g., TGFβ) to induce native cells to remodel the hydrogel.

Tissue and organ functions, particularly those under mechanical forces, are intrinsically linked with tissue composition and architecture [1,11]. Cartilaginous tissues, such as the IVD, need to resist various mechanical forces while remaining pliable enough to allow movement [1,11]. Collagen type 2 and Aggrecan are two cornerstones of IVD composition and function [1,11,40]. Immunohistochemistry staining for Collagen Type 2 and Aggrecan showed ample staining, primarily localized on the NP (Fig. 4c–iii,iv). TGFβ notably failed to induce significant recovery of either ECM component after injury (results mirrored in literature) [3]. While bare BIOGEL enabled modest recovery of Aggrecan synthesis, treatment with TGFβ-loaded BIOGEL promoted the greatest recovery of matrix (Aggrecan and Collagen type 2) synthesis (Fig. 4d–iii, iv). Holistic IVD evaluation using a histological grading scheme (details in literature reference) also corroborated the conclusion of enhanced tissue recovery when patients are treated with TGFβ-loaded BIOGEL (Fig. 4d–v) [24,40]. Taken together with H&E and Safranin O staining, our results provide ample evidence that TGFβ-loaded BIOGEL induced significant recovery of key histological features of the IVD, including key proteoglycans and structural proteins. Moreover, treatments with TGFβ solution or BIOGEL alone failed to produce consistent recovery.

Concurrent with tissue damage, IVD degeneration is associated with inflammation [41,42]. While numerous cells are involved in inflammation, macrophages (identified by Iba1) remain an integral mediator across many tissues [41,42]. M1 macrophages (CD86-positive) are associated with a pro-inflammatory state which can lead to further tissue damage, while M2 (CD163-positive) is associated with anti-inflammation and regenerative processes such as tissue remodeling and matrix deposition [41,42]. In injured IVD, a significant number of macrophages infiltrated the damaged tissue (Fig. S11). While TGFβ and bare BIOGEL resulted in a moderate decrease in macrophages, TGFβ-loaded BIOGEL treatment produced the greatest reduction. Notably, the difference in macrophage infiltration between TGFβ-loaded BIOGEL and healthy controls was not statistically significant.

2.4. BIOGEL enhances in vivo functional recovery

Functional recovery is the ultimate goal of treating IVD degeneration. For this, the regenerated IVD must have the load-bearing capacity of native IVD and an absence of IVD degeneration symptoms. The *in vivo* IVD degeneration model from Fig. 4 was employed here to characterize functional recovery (Fig. 5a).

The IVD's capacity to retain water can be considered as the culmination of various factors, including the health of the cells and the degree of proteoglycan present [11,40]. High water content is paramount to the viscoelastic properties of the IVD and effective load-bearing; progressive water loss indicates greater IVD degeneration (Fig. 5b) [11]. T2-weighted magnetic resonance imaging (T2-MRI) was employed to acquire coronal and axial images non-invasively to evaluate the water content of regenerated IVD on day 42 [40,43]. Healthy control IVD appeared as a bright signal under T2-weighted MRI (highlighted with yellow arrows) (Fig. 5c–i) [11,40,43]. Conversely, injured IVD showed a significantly darker signal against the surrounding tissue, indicating severe degeneration and water loss. While TGFβ and bare BIOGEL treatments showed T2-MRI images with moderate signal intensity at the center of the IVD, they exhibited significantly reduced area compared to the healthy control. In contrast, IVD treated with TGFβ-loaded BIOGEL resulted in the highest signal intensity and area out of the treatment cohorts, signifying the greatest water retention. When the T2-MRI images were graded, TGFβ was found to have negligible regeneration compared to the non-treated injury control (Fig. 5d–i). This is expected as the lost NP tissue from the nucleotomy is not replaced, and native cells must regenerate the tissue without a scaffold. Conversely, both BIOGEL and TGFβ-loaded BIOGEL resulted in significant recovery of T2 contrast, with TGFβ-loaded BIOGEL exhibiting more extensive water retention. While bare BIOGEL provided a well-hydrated scaffold for

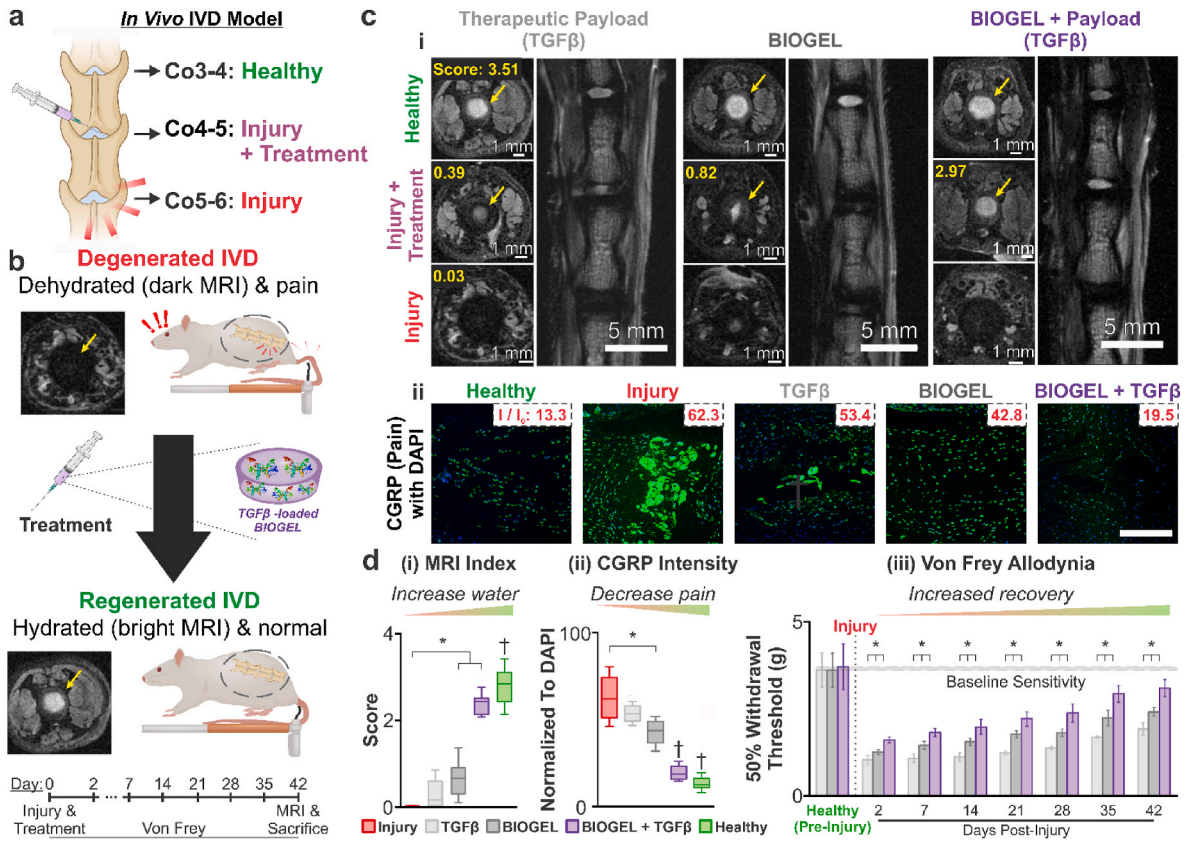

Fig. 5. Injectable TGFβ-loaded BIOGEL promotes IVD functional recovery after injury. a) Schematic diagram of *in vivo* IVD degeneration model. Nucleotomies were performed on the Co4-5 and Co5-6 IVD of Sprague-Dawley rats. Immediately after nucleotomies, treatments consisting of TGFβ solution, BIOGEL, and TGFβ-loaded BIOGEL were injected into the Co4-5 nucleus pulposus void space. Co3-4 IVD were monitored and used as a healthy control condition. **b)** Healthy IVD was defined by well-hydrated tissue (bright signal under T2-MRI) and lack of painful sensations under benign conditions (allodynia). **c) (i)** Coronal and axial images of the spine were taken with T2-MRI to measure water retention. Among treatment conditions, TGFβ-loaded BIOGEL led to the greatest recovery of bright T2 signal due to greater IVD hydration. **d) (i)** Grading for IVD MRI index revealed that treatment with bare BIOGEL and TGFβ-loaded BIOGEL resulted in significant recovery. **c) (ii)** Additionally, immunofluorescence staining for Calcitonin Gene Receptor Protein (CGRP) was performed to assess injury-induced pain. Injured IVD exhibited intense CGRP staining, which was mitigated in treated IVD. **d) (ii)** Quantification of CGRP staining against DAPI staining (cell nucleus) revealed that TGFβ-loaded BIOGEL induced significantly reduced pain compared to non-treated injuries and bare BIOGEL. **d) (iii)** Allodynia was assessed by measuring the amount of force (applied via Von Frey fibers) required to induce paw withdrawal in 50% of testing measurements. Starting two days post-treatment, rats with TGFβ-loaded BIOGEL hydrogels showed a greater withdrawal threshold compared to rats treated with TGFβ solution and bare BIOGEL, indicating greater recovery from allodynia. MRI index, relative CFRP intensity per DAPI, and 50% withdrawal threshold were analyzed using one-way ANOVA followed by Tukey's HSD [$\alpha = 0.05$; * indicates a statistically significant difference, † indicates a statistically significant difference against all other conditions with different symbols; treatments (CGRP and MRI): n = 4 biological replicates, healthy and injury: n = 12 biological replicates (i.e., 4 from each treatment group); treatments (Von Frey): n = 6].

remodeling, it lacked the cell signaling cues to initiate remodeling towards cartilage-like tissue. TGFβ-loaded BIOGEL contained both cell signaling cues and a physical scaffold for tissue remodeling, resulting in the greatest regeneration.

One of the principal clinical manifestations of IVD degeneration is back pain, which is responsible for a significant portion of healthcare and economic burden (e.g., high medical expenses and lost productivity) in developed countries [44]. Reducing pain caused by IVD degeneration is a key step towards functional recovery as it will allow patients to resume normal activities after the IVD has regenerated damaged tissue. Neuropathic pain such as allodynia can be caused by IVD degeneration, so mechanical allodynia was measured to assess discogenic back pain recovery in IVD degeneration. Von Frey filaments were used to test allodynia by measuring paw withdrawal threshold and allodynia, while the presence of sensory neuropeptide Calcitonin Gene Receptor Protein (CGRP) was assessed via immunofluorescence (Fig. 5b) [45,46]. Healthy IVD showed little staining for CGRP, while injured IVD showed abundant and intense CGRP (Fig. 5c–ii). Neither TGFβ nor bare BIOGEL treatments substantially reduced CGRP staining intensity (normalized to DAPI staining) (Fig. 5d–ii). Conversely, IVD treated with TGFβ-loaded BIOGEL showed significantly reduced CGRP staining intensity. These results indicate that encapsulating therapeutic payloads (e.g., TGFβ) in BIOGEL potentiated discogenic pain reduction. As predicted by the greater histological recovery in the preceding sections, animals treated with TGFβ-loaded BIOGEL displayed a greater tolerance to mechanical forces (i.e., probing with Von Frey filaments) before initiating an adverse reaction (e.g., paw withdrawal) (Fig. 5d–iii). This increased force/pain tolerance indicates less severe allodynia starting two days post-treatment, compared to animals treated with TGFβ or bare BIOGEL.

The ability to treat IVD degeneration-related allodynia indicates accelerated recovery from discogenic back pain and earlier resumption of normal activity for human patients [44]. This expedited treatment of IVD symptoms would alleviate strain on healthcare and social security systems by presenting an effective treatment for one of the leading causes of medical disabilities in adults [44].

3. Conclusions

In summary, we developed an injectable bioorthogonal hydrogel (BIOGEL) system for enhanced IVD tissue regeneration. More specifically, tetrazine and norbornene functional groups were grafted onto gelatin to produce a biocompatible, biodegradable, and cell adhesive

hydrogel that can crosslink *in situ*. The liquid GelTz and GelNb precursor solutions remained low viscosity across a wide range of temperatures, allowing for ergonomic injections and reducing shear stresses experienced by any encapsulated payloads. Once the liquid precursors were activated via simple mixing, a clinical operator was allowed a comfortable window of time to inject the solution (5–10 min) before it stabilized and formed a hydrogel that displayed biomechanical properties similar to healthy IVD tissue. To demonstrate synergy with existing growth factor therapies, the BIOGEL system was supplemented with TGFβ to provide a sustained release profile, which potentiated the anti-inflammatory and pro-regenerative effects of TGFβ in vitro. Moreover, TGFβ-loaded BIOGEL was administered to an *in vivo* rat model of IVD degeneration to induce greater histological recovery (e.g., recovered tissue architecture and induced de novo matrix synthesis) and functional recovery (e.g., increased water retention and reduced discogenic pain) than either TGFβ or BIOGEL component by itself. Since BIOGEL relies on bioorthogonal chemistry and utilizes gelatin derived from collagen (a major component of mammalian extracellular matrices), this system can be easily extended to include other payloads, target other degenerative conditions, and regenerate various tissues. In short, given BIOGEL's versatility in tissue engineering, we expect this technology platform will be applicable to a broad range of regenerative medicine and clinical conditions other than IVD regeneration.

4. Materials and methods

4.1. Materials

An exhaustive list of generic, non-trademarked chemicals of non-biological origin (e.g., formalin and DMEM/F-12) can be found in the **Supplementary Information**. Detailed synthesis procedures for tetrazine-methylamine, succinylated gelatin, gelatin-tetrazine (GelTz) and gelatin-norbornene (GelNb) are also included in the **Supplementary Information.**

Rompun® was purchased from Bayer. RapidCal™ Immuno was purchased from BBC Biochemical. Matrigel® were purchased from Corning. Sprague-Dawley rats were purchased from Orient Bio Inc. Berkovich silicon tips were purchased from Park Systems. Recombinant human FGF-basic (bFGF) was purchased from PeproTech. Complete Nucleus Pulposus Cell Media (CNPCM), human annulus fibrosus cells (hAFCs), and human nucleus pulposus cells (hNPCs) were purchased from ScienCell. B27™ Supplement, human transforming growth factor beta 3 (TGFβ3), lipopolysaccharide (LPS), N2™ Supplement, Neurobasal™ media, and PrestoBlue™ Cell Viability Reagent, was purchased from Thermo Fisher. Zoletil® was purchased from Virbac Laboratories.

Human induced pluripotent stem cell-derived neuronal progenitor cells (hiPSC-NPC) were a generous gift from Dr. Muoti (UC San Diego).

4.2. Precursor and hydrogel cytotoxicity

For precursor cytotoxicity with hAFCs and hNPCs, wells of a 96-well plate were coated with PLL as specified by ScienCell for hAFC and hNPC culture. Each well was seeded with hAFCs or hNPCs suspended in either GelTz in DPBS (5% w/v), GelNb in DPBS (5% w/v), or CNPCM (control) (400,000 cell mL^{-1}, 25 μL). After 15 min, CNPCM (200 μL) was added to each well.

For hydrogel cytotoxicity with hAFCs and hNPCs, wells of a 96-well plate were coated with either Matrigel® or BIOGEL (25 μL). Matrigel (4 °C) and BIOGEL in DPBS (5% w/v, used within 5 min of mixing) were pipetted into their respective wells and allowed to form hydrogels in a humidified, 37 °C incubator for at least 15 min before cell seeding. PLL-coated wells (prepared as specified by ScienCell for hAFC and hNPC culture) were used as a control. Each well was seeded with hAFCs or hNPCs (50,000 cell mL^{-1}, 200 μL) suspended in CNPCM.

For hydrogel cytotoxicity with hiPSC-NPC, Matrigel® and BIOGEL-coated wells were prepared as above. Diluted Matrigel®-coated wells (1:200 in DMEM/F-12) were used as a control. Each well was seeded with hiPSC-NPC (5000 cell mL^{-1}, 200 μL) suspended in proliferation media (0.5% B27, 0.5% N2, 20 ng mL^{-1} bFGF in 1:1 Neurobasal: DMEM/F-12).

For precursor cytotoxicity with hiPSC-NPC, wells of a 96-well plate were coated with diluted Matrigel®. Each well was seeded with hiPSC-NPC suspended in either GelTz in DPBS (5% w/v), GelNb in DPBS (5% w/v), or proliferation media (control) (5000 cell mL^{-1}, 25 μL). After 15 min, proliferation media (200 μL) was added to each well.

Cytotoxicity was assayed using PrestoBlue Cell Viability Reagent after 24-h culture with hydrogels or precursors. In brief, cells were washed with DPBS to remove excess uncrosslinked GelTz and GelNb before PrestoBlue in CNPCM or hiPSC-NPC proliferation media (10% v/v, 200 μL per well) was added. Wells without cells received PrestoBlue in CNPCM or hiPSC-NPC proliferation media for background correction. Plates were incubated in a humidified, 37 °C incubator and read using an Infinite M Plex plate reader (Tecan) according to manufacturer specification.

4.3. Field Emission-Scanning Electron Microscopy (FE-SEM) of Crosslinked Hydrogels

BIOGEL samples were formed using a standardized hydrogel mold. In short, Parafilm was placed over an empty pipette tip rack (5–200 μL, Fisher Scientific), and a multichannel pipette was used to create uniform divots. Equal volumes of hydrogel precursor solutions (25 μL each, 50 μL total) were mixed, pipetted into the molded divots to crosslink for 15 min. Crosslinked hydrogels were placed in a lyophilizer (Labconco) overnight to remove water.

Dehydrated samples were attached on SEM specimen mounts with carbon tape and coated with gold (20 nm thickness) using a sputter coater (Quorum Technologies). Electron microscopy was conducted using a secondary electron detector to form images with an FE-SEM (Carl Zeiss AG).

Cross-section samples were generated by cutting lyophilized BIOGEL samples with a stainless-steel razor blade and subjected to the same mounting and coating procedure as described above.

4.4. Rheometry

Rheological measurements were conducted with a Kinexus Ultra rotational rheometer (Malvern Instruments). Solutions (5% w/v, 200 μL distilled water) were loaded into a 600 μm gap between two flat, stainless-steel plates (top 20 mm diameter). GelTz-Nb precursors were mixed and pipetted directly on the rheometer to ensure the cross-linked hydrogel conforms to the top and bottom geometry gap.

Gelatin, SA-Gel, GelTz, GelNb, and GelTz-Nb hydrogel crosslinking were measured with an oscillatory time sweep at a constant 37 °C, 1 Hz, 1% shear strain for 100 min.

Crosslinked BIOGEL samples were subjected to the following tests: (1) an oscillatory frequency sweep at a constant 37 °C, 1% shear strain for 0.01–10 Hz and (2) an oscillatory amplitude sweep at a constant 37 °C, 1 Hz for 0.01–10% shear strain.

Gelatin, SA-Gel, GelTz and GelNb were subjected to the following tests: (1) a viscometry temperature sweep at a constant 1 and 100 s^{-1} for 37-4 °C and (2) an oscillatory temperature sweep at a constant 1 Hz, 1% shear strain for 37-4 °C.

4.5. Atomic force microscopy (AFM) of Crosslinked Hydrogels

A hydrophobic barrier pen was used to draw a sample retention square on a glass coverslip. Crosslinked hydrogels were placed in the middle of the square to prevent excessive hydrogel movement during microscopy.

AFM (Park Systems) was performed in contact mode with a Berkovich silicon tip at a scan rate of 0.5 Hz over a 5 × 5 μm area. The

hydrogel and probe were kept immersed in distilled water for the duration of probing. Young's modulus was calculated using XEI (Park Systems) software to apply the Oliver-Pharr Model across 10 randomly selected areas. This measurement process was repeated across 3 different regions to yield the reported hydrogel Young's modulus and standard deviation.

4.6. FITC-insulin release from BIOGEL

A blocking buffer (1% w/v) was prepared with bovine serum albumin in DPBS. A 24-well plate was pre-treated with blocking buffer (2 mL per well) and placed on a rotary shaker (75 rpm) overnight at 37 °C. The blocking buffer was replaced with DPBS (1.5 mL) immediately before use.

Gelatin-Tetrazine (GelTz) and Gelatin-Norbornene (GelNb) were dissolved in either DPBS or fluorescein isothiocyanate-labeled insulin (FITC-Insulin) in DPBS solution (0.25 mg mL^{-1}) with the aid of a sonicator bath to yield hydrogel precursor solutions (5% w/v). A hydrogel mold was made by spreading Parafilm over an empty pipette tip rack (5–200 μL, Fisher Scientific) and using a multichannel pipet to create uniform divots. Equal volumes of hydrogel precursor solutions (25 μL each, 50 μL total) were mixed, pipetted into the molded divots to crosslink for 15 min, and transferred to the pre-treated 24-well plate. The well plate was covered with aluminum foil and sealed with Parafilm before placement on a rotary shaker (75 rpm) set in a 37 °C incubator. An aliquot of FITC-Insulin solution was placed in a glass dram vial, covered with aluminum foil, and placed alongside the well plate for the duration of the experiment.

Fluorescence measurements were taken at 1 h, 4 h, 1 day, 2 d, 3 d, 1 week, and 2 wk using a plate reader (Tecan Infinite M200 Pro) at λ_{ex} = 488 nm, λ_{em} = 525 nm. An aliquot (100 μL) was taken from each well without replacement and placed in a half area, black well plate for fluorescence readings. A standard curve was created by serial dilution of the co-incubated FITC-Insulin solution at each time point to calculate % FITC-Insulin release.

4.7. In vitro TGFβ release for anti-inflammatory response

PLL-coated wells of a 24-well plate were seeded with hAFCs and hNPCs resuspended in CNPCM (200,000 cell mL^{-1}, 0.5 mL) and allowed to stabilize overnight. Likewise, Matrigel®-coated wells were seeded with hiPSC-NPC in proliferation media in a similar manner.

TGFβ3 was diluted in DPBS (0.15 mg mL^{-1}) before addition to GelTz in DPBS (5% w/v) for a final concentration of 75 μg mL^{-1} TGFβ3 (TGFβ3 + GelTz). TGFβ3 was excluded from the control unsupplemented BIOGEL; only DPBS was used to dilute the stock GelTz (5% w/v) solution.

Parafilm divots detailed in section "**4.3 Field Emission-Scanning Electron Microscopy (FE-SEM) of Crosslinked Hydrogels**" were employed. (TGFβ3 +) GelTz (16.56 μL) and GelNb (5% w/v, 12.5 μL) solutions were mixed and allowed to form hydrogels in the Parafilm divots at least 15 min prior to being introduced to cells.

hAFC and hNPC media was replaced with LPS-containing CNPCM (10 μg mL^{-1}, 0.6 mL) to simulate intervertebral disc degeneration. Likewise, hiPSC-NPC media was replaced with LPS-containing proliferation media at the same concentration. A cell culture insert (0.4 μm pore size, polycarbonate, 6.5 mm) was added to each well and filled with LPS-containing media (10 μg mL^{-1}, 0.1 mL). In non-LPS-containing controls, LPS was omitted from the media.

In control and TGFβ3-treated wells, DPBS or TGFβ3 (0.25 mg mL^{-1} TGFβ3, 2.5 μL) was added to the cell culture inserts. In (TGFβ3 +) BIOGEL-treated wells, appropriate hydrogels were transferred into the cell culture inserts. After 24 h, cell contents were harvested for RT-qPCR (see **Supplementary Information** for detailed protocol) with primers, as specified in Table S1.

4.8. Animal model for intervertebral disc (IVD) injury and treatment

All animal study procedures were approved by the Institutional Animal Care and Use Committee (IACUC) of CHA Bundang Medical Center (IACUC200141).

Eight-week-old Sprague-Dawley rats (220–240 g) were kept in a controlled environment (22 ± 1 °C, 50 ± 1% relative humidity, and 12/12 h light/dark cycle) for the duration of the study. Animals were anesthetized by intraperitoneal injection of Zoletil® (50 mg kg^{-1}) and Rompun® (10 mg kg^{-1}) before being placed on heated pads for the duration of surgery. The tail and pelvic area were sterilized with 70% alcohol, followed by povidone iodine. A skin incision (1 cm) was made longitudinally along the tail followed by the insertion of a scalpel blade (#11, 1.5 mm) into coccygeal discs Co4-5 and Co 5–6. The annulus fibrosus was longitudinally cut to expose the NP for nucleotomy via aspiration (22-gauge needle, 5 mL syringe). BIOGEL, TGFβ, and TGFβ-loaded BIOGEL (5% w/v in DPBS) were prepared and intradiscally injected into the Co 4–5 nucleotomy site (10 μL, 25-gauge catheter).

The surgical site was sutured and disinfected with povidone-iodine before subcutaneous injection of normal saline (0.9%, 5 mL). For 3 days post-surgery, animals were prophylactically treated with Cefazolin and Ketoprofen.

Twenty four Sprague Dawley rats were subjected to nucleotomies at coccygeal vertebrae 4–5 and 5–6 (Co4-5 and Co5-6), with Co4-5 receiving TGFβ, BIOGEL, or TGFβ-loaded BIOGEL treatments. Co3-4 was designated as the non-injured control. The rats were randomly divided into three groups: (1) TGFβ, (2) BIOGEL, and (3) TGFβ-loaded BIOGEL treatment groups (n = 8 for each group). Fourty two days after treatment, the coccygeal discs were removed for radiologic and histologic analysis.

4.9. Histological recovery assessments of IVD regeneration

Animals were sacrificed six weeks post-surgery to evaluate tissue structure and morphology. IVD and adjacent vertebral bodies were fixed in neutral buffered formalin (10%) for one week, decalcified with RapidCal Immuno for two weeks, paraffin-embedded, sliced using a microtome (Leica) to produce coronal sections (10 μm), dewaxed, and rehydrated.

Tissue architecture was determined by Safranin-O and Mayer's Hematoxylin & Eosin staining. Sections were mounted using mounting media and scanned with a microscope (OLYMPUS).

Built-in ImageJ region of interest functions were used to determine the NP area. Additionally, IVD tissue architecture was graded by blinded pathologists for the following criteria as detailed elsewhere (0 for healthy disc, 2 for severely injured disc): AF morphology (score 0–2), NP cellularity (score 0–2), NP matrix (score 0–2), and the boundary between AF and NP (score 0–2) [24]. The IVD tissue architecture score is presented as an average of the four criteria.

Specific markers were determined via immunostaining with antibodies, as specified in Table S2. Sectioned samples were incubated with primary antibodies at 4 °C for overnight, washed with DPBS and Tween 20, incubated with secondary antibodies at room temperature for 1 h, washed, and counter-stained with DAPI for 10 min. Sections were mounted using mounting media and scanned with a fluorescence microscope (Zeiss).

Built-in ImageJ region of interest functions were used to determine positive staining area and relative cell number percentages.

4.10. Functional recovery assessments of IVD regeneration

Von Frey tests were conducted −2 [pre-injury], 2, 7, 14, 21, 28, 35, and 42 days after surgery to assess mechanical allodynia as pain behavior in rats. Animals were placed into individual six-compartment enclosures with wire mesh floors and lids with air holes for a habituation period (20 min) to minimize exploratory activity. Von Frey hairs

(starting with a 2-g filament) were applied to the ventral surface of the tail base with sufficient force to buckle the filament. Positive responses were recorded if animals displayed flinching, licking, withdrawing, or tail shaking behaviors within 6 s of filament application. Tests were conducted five times for each rat with two blinded observers.

A T2-weighted, 9.4 T MRI spectrometer (Bruker BioSpec) was used to study the changes in disc structure and water content 42 days after surgery. T2-weighted MRI protocol was set as: (1) coronal plane; time to repetition (TR) of 5000 ms, time to echo (TE) of 30 ms, 150 horizontal x 150 vertical matrix; field of view of 15 horizontal_15 vertical, and 0.5 mm slices with 0 mm spacing between each slice. (2) Sagittal plane; time to repetition (TR) of 5000 ms (ms), time to echo (TE) of 50 ms, 200 horizontal_600 vertical matrix; field of view of 20 horizontal_60 vertical, and 0.8 mm slices with 0 mm spacing between each slice. The signal intensity and MRI index (the area of NP multiplied by average signal intensity) were evaluated [47]. Built-in ImageJ region of interest functions were used to determine the signal intensity (product of NP area and average signal intensity) while two blinded observers were used to determine the MRI index as detailed elsewhere [43].

4.11. Statistical analysis

In vitro RT-qPCR data was analyzed with R (statistical program), while *in vivo* data was analyzed with GraphPad Prism. All data are visualized as mean ± standard deviation. Statistical significance was defined as p-value < 0.05 when analyzed by one-way ANOVA followed by Tukey's HSD test.

4.12. Computer graphics

OriginLab was used for data analysis and graphing unless indicated otherwise. TGFβ and gelatin figures were obtained from RCSB PDB (PDB ID: 1TGK and 1BKV) and visualized using Mol* [48–52]. Select graphics were created with BioRender.com.

Funding

Ki-Bum Lee gratefully acknowledges the partial financial support from the NSF (CBET-1803517), the New Jersey Commission on Spinal Cord Research (CSCR17IRG010; CSCR22ERG023), SAS-Grossman Innovation Prize, and NIH R01 (1R01DC016612, 3R01DC016612-01S1, and 5R01DC016612-02S1). Inbo Han would like to acknowledge funding support from the Korea Health Technology Research and Development Project, Ministry for Health and Welfare Affairs (HR16C0002), and National Research Foundation of Korea (NRF-2020R1A2C4001870). Jeffrey Luo acknowledges the fellowship from the NIH T32 Biotechnology Training Fellowship (GM008339).

Human subjects

Human subjects were not used for this study nor were human tissues taken during this study. Cell lines were obtained from reputable commercial sources (ScienCell Research Laboratories, Inc.) and academic groups (Dr. Muoti, UC San Diego) who have received informed consent from donors or authorized agents.

IACUC approval obtained

All animal study procedures were approved by the Institutional Animal Care and Use Committee (IACUC) of CHA Bundang Medical Center (IACUC200141).

Animal welfare

All animal housing and experiments were conducted in strict accordance with the Institutional Animal Care and Use Committee (IACUC) of CHA Bundang Medical Center.

Data availability

The raw and processed data required to reproduce these findings are available from the corresponding authors upon request.

CRediT authorship contribution statement

Jeffrey Luo: Conceptualization, Methodology, Software, Validation, Formal analysis, Investigation, Resources, Data curation, Writing – original draft, Writing – review & editing, Visualization. **Anjani Darai:** Methodology, Software, Validation, Formal analysis, Investigation, Data curation, Writing – review & editing, Visualization. **Thanapat Pongkulapa:** Writing – review & editing, Visualization. **Brian Conley:** Conceptualization, Methodology. **Letao Yang:** Conceptualization, Writing – review & editing. **Inbo Han:** Supervision, Project administration, Funding acquisition. **Ki-Bum Lee:** Supervision, Project administration, Funding acquisition.

Declaration of competing interest

The authors declare that they have no known competing financial interests or personal relationships that could have appeared to influence the work reported in this paper.

Acknowledgements

The authors would like to acknowledge the Rutgers Graduate Writing Program for their assistance with manuscript prose and Prof. Jinho Yoon (Catholic University of Korea) for assistance with atomic force microscopy.

Appendix A. Supplementary data

Supplementary data to this article can be found online at https://doi.org/10.1016/j.bioactmat.2022.11.017.

References

[1] M.A. Adams, P.J. Roughley, What is intervertebral disc degeneration, and what causes it? Spine 31 (2006) 2151–2161.
[2] R.D. Bowles, L.A. Setton, Biomaterials for intervertebral disc regeneration and repair, Biomater. 129 (2017) 54–67.
[3] A.J. Walsh, D.S. Bradford, J.C. Lotz, In vivo growth factor treatment of degenerated intervertebral discs, Spine 29 (2004) 156–163, https://doi.org/10.1097/01.BRS.0000107231.67854.9F.
[4] L.M. Wakefield, T.S. Winokur, R.S. Hollands, K. Christopherson, A.D. Levinson, M. B. Sporn, Recombinant latent transforming growth factor beta 1 has a longer plasma half-life in rats than active transforming growth factor beta 1, and a different tissue distribution, J. Clin. Invest. 86 (1990) 1976–1984, https://doi.org/10.1172/Jci114932.
[5] K. Masuda, Biological repair of the degenerated intervertebral disc by the injection of growth factors, Eur. Spine J. 17 (2008) 441–451, https://doi.org/10.1007/s00586-008-0749-z.
[6] J. Li, D.J. Mooney, Designing hydrogels for controlled drug delivery, Nat. Rev. Mater. 1 (2016) 1–17, https://doi.org/10.1038/natrevmats.2016.71.
[7] J.M. Alonso, J. Andrade del Olmo, R. Perez Gonzalez, V. Saez-Martinez, Injectable hydrogels: from laboratory to industrialization, Polymers 13 (2021) 650, https://doi.org/10.3390/polym13040650.
[8] J.H. Lee, Injectable hydrogels delivering therapeutic agents for disease treatment and tissue engineering, Biomater. Res. 22 (2018) 1–14, https://doi.org/10.1186/s40824-018-0138-6.
[9] N. Annabi, J.W. Nichol, X. Zhong, C. Ji, S. Koshy, A. Khademhosseini, F. Dehghani, Controlling the porosity and microarchitecture of hydrogels for tissue engineering, Tissue Eng. B Rev. 16 (2010) 371–383, https://doi.org/10.1089/ten.TEB.2009.0639.
[10] S.T. Koshy, R.M. Desai, P. Joly, J. Li, R.K. Bagrodia, S.A. Lewin, N.S. Joshi, D. J. Mooney, Click-crosslinked injectable gelatin hydrogels, Adv. Healthcare Mater. 5 (2016) 541–547, https://doi.org/10.1002/adhm.201500757.
[11] B.V. Fearing, P.A. Hernandez, L.A. Setton, N.O. Chahine, Mechanotransduction and cell biomechanics of the intervertebral disc, JOR spine 1 (2018) e1026, https://doi.org/10.1002/jsp2.1026.

[12] R.F. Heary, N. Parvathreddy, S. Sampath, N. Agarwal, Elastic modulus in the selection of interbody implants, J. Spine Surg. 3 (2017) 163, https://doi.org/10.21037/jss.2017.05.01.

[13] C.-Y. Lin, H. Kang, J.P. Rouleau, S.J. Hollister, F. La Marca, Stress analysis of the interface between cervical vertebrae end plates and the Bryan, Prestige LP, and ProDisc-C cervical disc prostheses: an in vivo image-based finite element study, Spine 34 (2009) 1554–1560, https://doi.org/10.1097/BRS.0b013e3181aa643b.

[14] J.J. Rawlinson, K.P. Punga, K.L. Gunsallus, D.L. Bartel, T.M. Wright, Wear simulation of the ProDisc-L disc replacement using adaptive finite element analysis, J. Neurosurg. Spine 7 (2007) 165–173, https://doi.org/10.3171/Spi-07/08/166.

[15] M.D. Harmon, D.M. Ramos, D. Nithyadevi, R. Bordett, S. Rudraiah, S. P. Nukavarapu, I.L. Moss, S.G. Kumbar, Growing a backbone–functional biomaterials and structures for intervertebral disc (ivd) repair and regeneration: challenges, innovations, and future directions, Biomater. Sci. 8 (2020) 1216–1239, https://doi.org/10.1039/c9bm01288e.

[16] J. Stergar, L. Gradisnik, T. Velnar, U. Maver, Intervertebral disc tissue engineering: a brief review, Bosn. J. Basic Med. Sci. 19 (2019) 130, https://doi.org/10.17305/bjbms.2019.3778.

[17] S. van Uden, J. Silva-Correia, J.M. Oliveira, R.L. Reis, Current strategies for treatment of intervertebral disc degeneration: substitution and regeneration possibilities, Biomater. Res. 21 (2017) 1–19, https://doi.org/10.1186/s40824-017-0106-6.

[18] J. Zhu, R.E. Marchant, Design properties of hydrogel tissue-engineering scaffolds, Expet Rev. Med. Dev. 8 (2011) 607–626, https://doi.org/10.1586/erd.11.27.

[19] J. Van Hoorick, L. Tytgat, A. Dobos, H. Ottevaere, J. Van Erps, H. Thienpont, A. Ovsianikov, P. Dubruel, S. Van Vlierberghe, (Photo-) crosslinkable gelatin derivatives for biofabrication applications, Acta Biomater. 97 (2019) 46–73, https://doi.org/10.1016/j.actbio.2019.07.035.

[20] A.B. Bello, D. Kim, D. Kim, H. Park, S.-H. Lee, Engineering and functionalization of gelatin biomaterials: from cell culture to medical applications, Tissue Eng. B Rev. 26 (2020) 164–180.

[21] D.M. Patterson, L.A. Nazarova, J.A. Prescher, Finding the right (bioorthogonal) chemistry, ACS Chem. Biol. 9 (2014) 592–605, https://doi.org/10.1021/cb400828a.

[22] A. Sivashanmugam, R.A. Kumar, M.V. Priya, S.V. Nair, R. Jayakumar, An overview of injectable polymeric hydrogels for tissue engineering, Eur. Polym. J. 72 (2015) 543–565, https://doi.org/10.1016/j.eurpolymj.2015.05.014.

[23] M.H. Amer, F.R. Rose, K.M. Shakesheff, M. Modo, L.J. White, Translational considerations in injectable cell-based therapeutics for neurological applications: concepts, progress and challenges, NPJ Regener. Med. 2 (2017) 1–13, https://doi.org/10.1038/s41536-017-0028-x.

[24] K. Masuda, Y. Aota, C. Muehleman, Y. Imai, M. Okuma, E.J. Thonar, G. B. Andersson, H.S. An, A novel rabbit model of mild, reproducible disc degeneration by an anulus needle puncture: correlation between the degree of disc injury and radiological and histological appearances of disc degeneration, Spine 30 (2005) 5–14, https://doi.org/10.1097/01.brs.0000148152.04401.20.

[25] Y. Saruhashi, K. Mori, A. Katsuura, S. Takahashi, Y. Matsusue, S. Hukuda, Evaluation of standard nucleotomy for lumbar disc herniation using the Love method: results of follow-up studies after more than 10 years, Eur. Spine J. 13 (2004) 626–630, https://doi.org/10.1007/s00586-004-0690-8.

[26] J. Chin, K. Lang, in: W.I.P. Organization (Ed.), Methods of Incorporating an Amino Acid Comprising a Bcn Group into a Polypeptide Using an Orthogonal Codon Encoding it and an Orthorgonal Pylrs Synthase, Medical Research Council, 2013.

[27] D.P. Pioletti, Integration of mechanotransduction concepts in bone tissue engineering, Comput. Methods Biomech. Biomed. Eng. 16 (2013) 1050–1055, https://doi.org/10.1080/10255842.2013.780602.

[28] L. Cacopardo, N. Guazzelli, A. Ahluwalia, Characterizing and Engineering Biomimetic Materials for Viscoelastic Mechanotransduction Studies, 2021, https://doi.org/10.1089/ten.TEB.2021.0151. Tissue Engineering Part B: Reviews.

[29] S. Umehara, S. Tadano, K. Abumi, K. Katagiri, K. Kaneda, T. Ukai, Effects of degeneration on the elastic modulus distribution in the lumbar intervertebral disc, Spine 21 (1996) 811–819, https://doi.org/10.1097/00007632-199604010-00007.

[30] J.C. Iatridis, L.A. Setton, M. Weidenbaum, V.C. Mow, Alterations in the mechanical behavior of the human lumbar nucleus pulposus with degeneration and aging, J. Orthop. Res. 15 (1997) 318–322, https://doi.org/10.1002/jor.1100150224.

[31] E.-Y. Kim, B.-C. Kim, Lipopolysaccharide inhibits transforming growth factor-beta1-stimulated Smad6 expression by inducing phosphorylation of the linker region of Smad3 through a TLR4–IRAK1–ERK1/2 pathway, FEBS Lett. 585 (2011) 779–785, https://doi.org/10.1016/j.febslet.2011.01.044.

[32] W. Li, T. Liu, L. Wu, C. Chen, Z. Jia, X. Bai, D. Ruan, Blocking the function of inflammatory cytokines and mediators by using IL-10 and TGF-β: a potential biological immunotherapy for intervertebral disc degeneration in a beagle model, Int. J. Mol. Sci. 15 (2014) 17270–17283.

[33] H. Yang, C. Cao, C. Wu, C. Yuan, Q. Gu, Q. Shi, J. Zou, TGF-βl suppresses inflammation in cell therapy for intervertebral disc degeneration, Sci. Rep. 5 (2015) 1–10.

[34] N.E. Rajan, O. Bloom, R. Maidhof, N. Stetson, B. Sherry, M. Levine, N.O. Chahine, Toll-Like Receptor 4 (TLR4) expression and stimulation in a model of intervertebral disc inflammation and degeneration, Spine 38 (2013) 1343–1351.

[35] T. Ohnishi, N. Iwasaki, H. Sudo, Causes of and molecular targets for the treatment of intervertebral disc degeneration: a review, Cells 11 (2022) 394.

[36] K. Phillips, K. Cullen, N. Chiverton, A. Michael, A. Cole, L. Breakwell, G. Haddock, R. Bunning, A. Cross, C. Le Maitre, Potential Roles of Cytokines and Chemokines in Human Intervertebral Disc Degeneration: Interleukin-1 Is a Master Regulator of Catabolic Processes, Osteoarthritis and Cartilage, 23, 2015, pp. 1165–1177, https://doi.org/10.1016/j.joca.2015.02.017.

[37] F.-J. Lyu, H. Cui, H. Pan, K. Mc Cheung, X. Cao, J.C. Iatridis, Z. Zheng, Painful intervertebral disc degeneration and inflammation: from laboratory evidence to clinical interventions, Bone Res 9 (2021) 1–14, https://doi.org/10.1038/s41413-020-00125-x.

[38] P.J. McKeown-Longo, P.J. Higgins, Integration of canonical and noncanonical pathways in TLR4 signaling: complex regulation of the wound repair program, Adv. Wound Care 6 (2017) 320–329, https://doi.org/10.1089/wound.2017.0736.

[39] T. Kluba, T. Niemeyer, C. Gaissmaier, T. Gründer, Human anulus fibrosis and nucleus pulposus cells of the intervertebral disc: effect of degeneration and culture system on cell phenotype, Spine 30 (2005) 2743–2748, https://doi.org/10.1097/01.brs.0000192204.89160.6d.

[40] S. Lim, S.B. An, M. Jung, H.P. Joshi, H. Kumar, C. Kim, S.Y. Song, J.R. Lee, M. Kang, I. Han, Local delivery of senolytic drug inhibits intervertebral disc degeneration and restores intervertebral disc structure, Adv. Healthcare Mater. 11 (2022), 2101483.

[41] K.R. Nakazawa, B.A. Walter, D.M. Laudier, D. Krishnamoorthy, G.E. Mosley, K. L. Spiller, J.C. Iatridis, Accumulation and localization of macrophage phenotypes with human intervertebral disc degeneration, Spine J. 18 (2018) 343–356, https://doi.org/10.1016/j.spinee.2017.09.018.

[42] A. Kawakubo, K. Uchida, M. Miyagi, M. Nakawaki, M. Satoh, H. Sekiguchi, Y. Yokozeki, G. Inoue, M. Takaso, Investigation of resident and recruited macrophages following disc injury in mice, J. Orthop. Res. 38 (2020) 1703–1709, https://doi.org/10.1002/jor.24590.

[43] C.W. Pfirrmann, A. Metzdorf, M. Zanetti, J. Hodler, N. Boos, Magnetic resonance classification of lumbar intervertebral disc degeneration, Spine 26 (2001) 1873–1878, https://doi.org/10.1097/00007632-200109010-00011.

[44] A.L. Dutmer, H.R.S. Preuper, R. Soer, S. Brouwer, U. Bültmann, P.U. Dijkstra, M. H. Coppes, P. Stegeman, E. Buskens, A.D. van Asselt, Personal and societal impact of low back pain: the Groningen spine cohort, Spine 44 (2019) E1443–E1451, https://doi.org/10.1097/BRS.0000000000003174.

[45] T. Ozawa, S. Ohtori, G. Inoue, Y. Aoki, H. Moriya, K. Takahashi, The degenerated lumbar intervertebral disc is innervated primarily by peptide-containing sensory nerve fibers in humans, Spine 31 (2006) 2418–2422.

[46] S.R. Chaplan, F.W. Bach, J. Pogrel, J. Chung, T. Yaksh, Quantitative assessment of tactile allodynia in the rat paw, J. Neurosci. Method. 53 (1994) 55–63.

[47] U.Y. Choi, H.P. Joshi, S. Payne, K.T. Kim, J.W. Kyung, H. Choi, M.J. Cooke, S. Y. Kwon, E.J. Roh, S. Sohn, M.S. Shoichet, I. Han, An Injectable Hyaluronan–Methylcellulose (HAMC) Hydrogel combined with Wharton's jelly-derived mesenchymal Stromal cells (WJ-MSCs) promotes degenerative disc repair, Int. J. Mol. Sci. 21 (2020) 7391.

[48] P.R. Mittl, J.P. Priestle, M.G. Gruetter, Human Transforming Growth Factor Beta 3, Crystallized from PEG 4000, 1996.

[49] P.R. Mittl, J.P. Priestle, D.A. Cox, G. Mcmaster, N. Cerletti, M.G. Grütter, The crystal structure of TGF-β3 and comparison to TGF-β2: implications for receptor binding, Protein Sci. 5 (1996) 1261–1271.

[50] R.Z. Kramer, J. Bella, P. Mayville, B. Brodsky, H.M. Berman, Sequence dependent conformational variations of collagen triple-helical structure, Nat. Struct. Biol. 6 (1999) 454–457, https://doi.org/10.1038/8259.

[51] R.Z. Kramer, J. Bella, P. Mayville, B. Brodsky, H.M. Berman, Collagen (1998).

[52] D. Sehnal, S. Bittrich, M. Deshpande, R. Svobodová, K. Berka, V. Bazgier, S. Velankar, S.K. Burley, J. Koča, A.S. Rose, Mol* Viewer: modern web app for 3D visualization and analysis of large biomolecular structures, Nucleic Acids Res. 49 (2021) W431–W437, https://doi.org/10.1093/nar/gkab314.